

# Learning to Recognize Objects by Retaining other Factors of Variation

Anonymous WACV submission

Paper ID 295

## Abstract

*Most ConvNets formulate object recognition from natural images as a single task classification problem, and attempt to learn features useful for object categories, but invariant to other factors of variation such as pose and illumination. They do not explicitly learn these other factors; instead, they usually discard them by pooling and normalization. Here, we take the opposite approach: we train ConvNets for object recognition by retaining other factors (pose in our case) and learning them jointly with object category. We design a new multi-task learning (MTL) ConvNet, named disentangling CNN (disCNN), which explicitly enforces the disentangled representations of object identity and pose, and is trained to predict object categories and pose transformations. disCNN achieves significantly better object recognition accuracies than the baseline CNN trained solely to predict object categories on the iLab-20M dataset, a large-scale turntable dataset with detailed pose and lighting information. We further show that the pre-trained features on iLab-20M generalize to both Washington RGB-D and ImageNet datasets, and the pretrained disCNN features are significantly better than the pretrained baseline CNN features for fine-tuning on ImageNet.*

## 1. Introduction

Images are generated under factors of variation, including pose, illumination etc. Recently, deep ConvNet architectures learn rich and high-performance features by leveraging millions of labelled images. They have achieved state-of-the-art object recognition performance. Contemporary CNNs, such as AlexNet [15], VGG [25], GoogLeNet [28] and ResNet [10], pose object recognition as a single task learning problem, and learn features that are sensitive to object categories but invariant to other nuisance information (e.g., pose and illumination) [26] as much as possible. To achieve this, current CNNs usually stack several stages of subsampling/pooling [19] and apply normalization operations [15, 14] to make representations invariant to small pose variations and illumination changes. However, as ar-

gued by Hinton et al [12], to recognize objects, neural networks should use “capsules” to encode both identity and other instantiation parameters (including pose, lighting and shape deformations). In [2, 21], authors argue as well that image understanding is to tease apart these factors, instead of emphasizing one and disregarding the others.

In this work, we formulate object recognition as a multi-task learning (MTL) problem by taking images as inputs and learning both object categories and other image generating factors (pose in our case) simultaneously. Thanks to the availability of both identity and 3D pose labels in the iLab-20M dataset of 22 million images of objects shot on a turntable, we use object identity and pose during training, and then investigate further generalization to other datasets which lack pose labels (Washington RGB-D and ImageNet). Contrary to the usual way to learn representations invariant to pose changes, we take the opposite approach by retaining the pose information and learning it jointly with object identities during the training process.

We leverage the power of ConvNets for high performance representation learning, and build our MTL framework on it. Concretely, our architecture is a two-streams ConvNet which takes a pair of images as inputs and predicts both the object category and the pose transformation between the two images. Both streams share the same CNN architecture (e.g., AlexNet) with the same weights and the same operations on each layer. Each stream independently extracts features from one image. In the top layer, we explicitly partition the representation units into two groups, with one group representing object identity and the other its pose. Object identity representations are passed down to predict object categories, while two pose representations are concatenated to predict the pose transformation between images (Fig. 1). By explicitly partitioning the top CNN layer units into groups, we learn the ConvNet in a way such that each group extracts features useful for its own task and explains one factor of variation in the image. We refer our architecture as disentangling CNN (disCNN), with disentangled representations for identity and pose.

During training, disCNN takes a pair of images as inputs, and learns features by using both object categories and

pose-transformations as supervision. The goal of disCNN is to recognize objects, therefore, in test, we take only one stream of the trained disCNN, use it to compute features for the test image, and only the identity representations in top layer are used and fed into the object category layer for categorization. In other words, pose representations are not used in test, and the pose-transformation prediction task in the training is auxiliary to the object recognition task, but essential for better feature learning.

## 2. Related work

ConvNets: over the past several years, convolutional neural networks [19] have pushed forward the state-of-the-art in many vision tasks, including image classification [15, 25, 28, 10], object detection [23, 7], image segmentation [4, 20], activity recognition [24, 8], etc. These tasks leverage the power of CNNs to learn rich features useful for the target tasks, and [1] show features learned by CNNs on one task can be generalized to other tasks. We aim to learn feature representations for different image generating factors, and we employ ConvNets as our building base.

Multitask learning: several efforts have explored multitask learning using deep neural networks, for face detection, phoneme recognition, and scene classification [22, 32, 31, 13]. All of them use a similar linear feed-forward architecture, with all task label layers directly appended onto the top layer. In the end, all tasks in these applications share the same representations. More recently, Su et al [27] use a CNN to estimate the camera viewpoint of the input image. They pose their problem as MTL by assuming that viewpoint estimate is object-class-dependent, and stack class-specific viewpoint layers onto the top of CNN. Our work differs from the above in that: we use two-stream CNNs and we explicitly partition the top layer representation into groups, with each group representing one task; therefore we have task-exclusive representations while in above works, all tasks share the same top layer representations.

Disentangling: As argued by Bengio [2], one of the key challenge to understanding images is to disentangle different factors, e.g. shape, texture, pose and illumination, that generate natural images. Reed et al [21] proposed the disentangling Boltzmann Machine (disBMs), which augments the regular RBM by partitioning the hidden units into distinct factors of variation and modelling their high-order interactions. In [33], the authors build a stochastic multi-view perceptron to factorize the face identity and its view representations by different sets of neurons, in order to achieve view-invariant face recognition. Our work is similar to the above two in that we explicitly partition the representations into distinct groups to force different factors disentangled; however, our model is deterministic and scales to large datasets, while the above methods are restricted to small datasets and often require expensive sampling inferences.

Dosovitskiy et al [6] proposed to use CNN to generate images of objects given object style, viewpoint and color. Their model essentially learns to simulate the graphics rendering process, but does not directly apply to image interpretation. Kulkarni et al [16] presented the Inverse Graphics Network (IGN), an encoder-decoder that learns to generate new images of an object under varying poses and lighting. The encoder of IGN learns a disentangled representation of transformations including pose, light and shape. Yang et al [30] proposed a recurrent convolutional encoder-decoder network to render 3D views from a single image. They explicitly split the top layer representations of the encoder into identity and pose units. Our work is similar to [16, 30] by using distinct units to represent different factors, but we differ in that: (1) our architecture is a MTL CNN which maps images to discrete labels, while theirs are autoencoders mapping images to images; (2) our model directly applies to large numbers of categories with complex images, but [16, 30] only tested their models on face and chair datasets with pure backgrounds.

Our work is most similar to [1], which shows that freely available egomotion data of mobile agents provides as good supervision as the expensive class-labels for CNNs to learn useful features for different vision tasks. Here, we use stereo-pairs of images as inputs to learn the camera motions as well, however, we are different in: (1) our architecture is a MTL framework, in which the task of camera-motion (pose-transformation) prediction serves as an auxiliary task to help object recognition; (2) our network is more flexible, which could take in both one image or a stereo-pair; (3) our MTL disCNN learns much better features for object-recognition than the baseline CNN using only class-label as supervision, while their single task two-streams CNNs only learn comparable features.

## 3. Method

Object identity is here defined to be the identity of one instance. Distinct instances, no matter whether they belong to the same class, have different object identities. Object pose refers to the extrinsic parameters of the camera taking the image, but given a single natural image taken by a consumer camera, it is hard to obtain the camera extrinsics, therefore the ground-truth object poses are expensive and sometimes impossible to collect in real cases. Camera extrinsics are known when we render 2D images from 3D models[27], but rendered 2D images are very different from natural images. Although single camera extrinsics are hard to get in real cases, the relative translation and orientation (a.k.a camera motion), represented by an essential matrix  $E$ , between a pair of images is relatively easier to compute, e.g., for calibrated cameras, first find 8 pairs of matched points, then use the normalized 8-point algorithm [9] to estimate. The camera motion between an image pair

162  
163  
164  
165  
166  
167  
168  
169  
170  
171  
172  
173  
174  
175  
176  
177  
178  
179  
180  
181  
182  
183  
184  
185  
186  
187  
188  
189  
190  
191  
192  
193  
194  
195  
196  
197  
198  
199  
200  
201  
202  
203  
204  
205  
206  
207  
208  
209  
210  
211  
212  
213  
214  
215

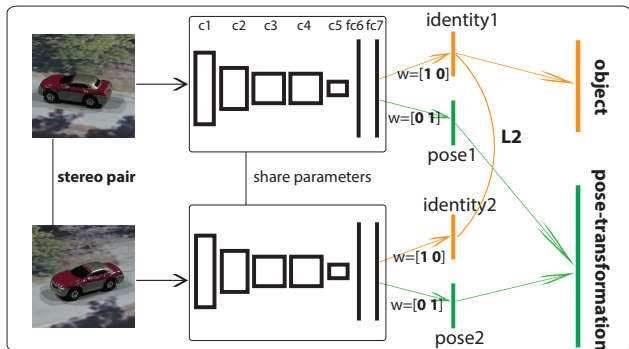


Figure 1. Architecture of our disentangling CNN (disCNN). disCNN is a two-streams CNN, which takes in an image pair and learns to predict the object category and the pose transformation jointly. In experiments, we use AlexNet in both streams to extract features, and explicitly partition the top layer representations fc7 into two groups: identity and pose. We further enforce two identity representations to be similar, and one identity representation is used for object category prediction, and two pose representations are concatenated to predict the pose transformation.

captures the pose transformation between objects in the two images. We use the relative pose transformation between objects instead of absolute object pose, as supervision. In the following, we use “pose transformation” and “camera motion” interchangeably.

Our system is designed to estimate any numeric pose transformations, but in experiments, we have a limited number of camera-pairs, with motion between each pair fixed. Therefore, we could further discretize the pose transformation using the fact that every image-pair taken under the same camera-pair has the same pose transformation, and the number of the camera-pairs determines the number of discrete pose-transformations. In this way, “pose transformation” estimation is transformed into a classification problem - classifying which camera-pair took the image-pair, with the number of labels equal to the number of camera-pairs.

### 3.1. Network Architecture

Our ultimate goal is to learn object identity representations for object recognition, but we further simultaneously learn the object pose transformation as an auxiliary task. Building a ConvNet that can predict the pose transformation between a stereo-pair of images is straightforward: the ConvNet should take the pair as input, after several layers of convolutions, it produces an output which assigns a probability to each camera-pair under which that image-pair could be taken. But note that the image-pair contains the same object instance taken under different camera viewpoints, we wish to learn an object identity representation, such that the same pair should have as similar object identity representations as possible.

We build a two-stream CNN architecture shown in Fig.

1, named disentangling CNN (disCNN). Each stream is a ConvNet independently extracting features from one image, and both ConvNets have the same architecture and share the same weights. Here we use AlexNet [15] as the ConvNet, but with faster GPUs one could use VGG [25] and GoogLeNet [28] as well. After getting fc7 representations, we explicitly partition the fc7 units into two groups, with one group representing object identity and the other representing object pose in a single image. Since object instances in an image pair are the same, we enforce the two identity representations to be similar by penalizing their  $\ell_2$ -norm differences, i.e.  $\|id_1 - id_2\|_2$ , where  $id_1$  and  $id_2$  are identity representations of two stereo images. One identity representation (either  $id_1$  or  $id_2$ ) is further fed into object-category label layer for object-category prediction. Two pose representations,  $pose_1$  and  $pose_2$ , are fused to predict the relative pose transformation, i.e., under which camera-pair the image-pair is taken. Our objective function is therefore the summation of two soft-max losses and one  $\ell_2$  loss:

$$\mathcal{L} = \mathcal{L}(object) + \lambda_1 \mathcal{L}(pose\ transformation) + \lambda_2 \|id_1 - id_2\|_2 \quad (1)$$

We follow AlexNet closely, which takes a  $227 \times 227$  image as input, and has 5 convolutional layers and 2 fully connected layers. ReLU non-linearities are used after every convolutional/fully-connected layer, and dropout is used in both fully connected layers, with dropout rate 0.5. The only change we make is to change the number of units on both fc6 and fc7 from 4096 to 1024, and one half of the units (512) are used to represent identity and the other half to represent pose. If we use abbreviations Cn, Fn, P, D, LRN, ReLU to represent a convolutional layer with n filters, a fully connected layer with n filters, a pooling layer, a dropout layer, a local response normalization layer and a ReLU layer, then the AlexNet-type architecture used in our experiments is: C96-P-LRN-C256-P-LRN-C384-C384-C256-P-F1024-D-F1024-D (we omit ReLU to avoid cluttering). If not explicitly mentioned, this is the baseline architecture for all experiments.

Notes: (1) the proposed two-stream CNN architecture is quite flexible in that: it could either take a single image or an image-pair as inputs. For a single image input, no pose transformation label is necessary, while for an image-pair input, it is not required to have an object-category label. For a pair of images without the object label, its loss reduces to two terms:  $\lambda_1 \mathcal{L}(pose - transformation) + \lambda_2 \|id_1 - id_2\|_2$ , the soft-max loss of the predicted pose-transformation and the  $\ell_2$  loss of two identity representations. Given a single image with a object label, the loss incurred by it reduces to only one term: the soft-max loss of the predicted category label  $\mathcal{L}(object)$ .

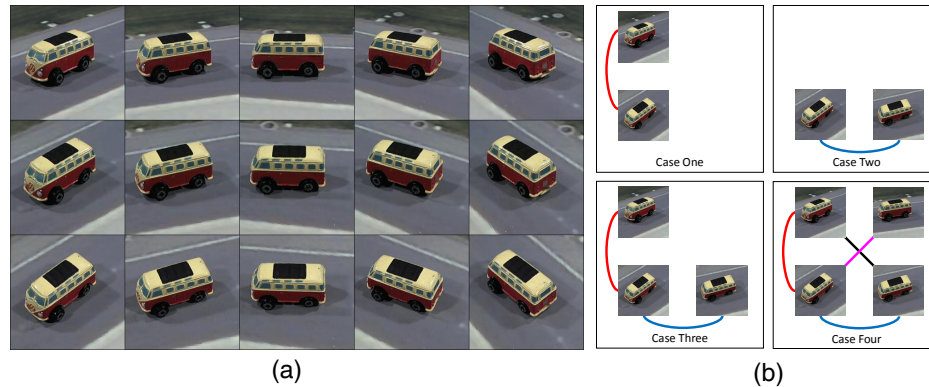


Figure 2. Exemplar iLab-20M images and camera pairs. (a) images of the same object instance taken by different cameras under different rotations, each row is taken under the same camera under different rotations, and each column is taken by different cameras under the same rotation; (b) camera pairs used in experiments.

(2) Scaling the same image-pair by different scales does not change its pose transformation label. In our case, each camera-pair has a unique essential matrix (up to some scale), and defines one pose-transformation label. By up/down scaling both images in a pair, the estimated essential matrix differs only by a scale factor. Since the essential matrix estimated from the raw image-pair is already uncertain up to a scale factor (e.g. using the eight-point method for estimation [9]), the essential matrix estimated from the scaled pairs is equivalent to that estimated from the raw pair. This is useful when objects have large scale differences: we could scale them differently to make them have similar scales (see experiments on Washington RGB-D dataset).

## 4. Experiments

In experiments, we first show the effectiveness of disCNN for object recognition against AlexNet on both iLab-20M and Washington RGB-D datasets. We further demonstrate that the pretrained disCNN on the iLab-20M dataset learns useful features for object recognition on the ImageNet dataset [5]: a AlexNet initialized with disCNN weights performs significantly better than a AlexNet initialized with random Gaussian weights.

### 4.1. iLab-20M dataset

The iLab-20M dataset [3] is a controlled, parametric dataset collected by shooting images of toy vehicles placed on a turntable using 11 cameras at different viewingpoints. There are totally 15 object categories with each object having 25~160 instances. Each object instance was shot on more than 14 backgrounds (printed satellite images), in a relevant context (e.g., cars on roads, trains on railtracks, boats on water). In total, 1,320 images were captured for each instance and background combinations: 11 azimuth

angles (from the 11 cameras), 8 turntable rotation angles, 5 lighting conditions, and 3 focus values (-3, 0, and +3 from the default focus value of each camera). The complete dataset consists of 704 object instances, with 1,320 images per object-instance/background combination, or almost 22M images.

Training and test instances: we use 10 (out of 15) object categories in our experiments (Fig. 4), and, within each category, we randomly choose 3/4 instances as training and the remaining 1/4 instances for testing. Under this partition, instances in test are never seen during training.

Image-pairs: we only take images shot under one fixed lighting condition (with all 4 lights on) and camera focus (focus = 0), but all 11 camera azimuths and all 8 turntable rotations as training and test images, equivalent to 88 virtual cameras on a semi-sphere. In principle, we can take image-pairs taken under any camera-pairs (e.g. any pair from  $C_{88}^2$  combinations), however, one critical problem is that image-pairs taken under camera-pairs with large viewpoint differences have little overlap, which makes it difficult, or even impossible to predict the pose-transformation (e.g., difficult to estimate the essential matrix). Therefore, in experiments, we only consider image-pairs taken by neighboring-camera pairs. All image-pairs shot under a fixed camera-pair share the same pose-transformation label, and finally the total number of pose-transformation labels is equal to the number of camera-pairs. In experiments, we consider different numbers of camera-pairs, and evaluate the influence on the performance of disCNN.

Fig. 2 shows images of one instance shot under different cameras and rotations: each row is shot by the same camera under different turntable rotations, and each column is shot by different cameras under the same turntable rotation. In experiments, we use different numbers of camera-pairs as supervision, therefore, only take image-pairs shot under the chosen camera-pairs as training. Case

378  
379  
380  
381  
382  
383  
384  
385  
386  
387  
388  
389  
390  
391  
392  
393  
394  
395  
396  
397  
398  
399  
400  
401  
402  
403  
404  
405  
406  
407  
408  
409  
410  
411  
412  
413  
414  
415  
416  
417  
418  
419  
420  
421  
422  
423  
424  
425  
426  
427  
428  
429  
430  
431

# of camera pairs	7	11	18	56
AlexNet	79.07	78.89	79.60	79.25
disCNN	<b>81.30</b>	<b>83.66</b>	<b>83.60</b>	<b>83.66</b>

Table 1. Object recognition accuracies (%) of AlexNet and disCNN on the iLab-20M dataset. disCNN consistently outperforms AlexNet under different numbers of camera pairs used as supervision, showing the advantage of jointly learning object identity and its pose. We see as well: disCNN performs better when more camera-pairs are used, e.g., the performance of disCNN increases by 2% when  $\geq 11$  camera pairs are used, compared with 7 camera pairs.

one (Fig. 2 (a) topleft): we take two neighboring cameras as one camera-pair (we skip 1 camera, i.e.,  $C_i - C_{i+2}$  is a camera-pair), resulting in 7 camera-pairs, therefore 7 pose-transformation labels. Image pairs taken by the same camera-pair under different rotations share the same pose-transformation label. Case two (Fig. 2 (b) topright): two images taken by one camera under two adjacent rotations ( $(C_i R_j, C_i R_{j+1})$ ) can be imagined to be taken by a pair of virtual cameras, resulting in 11 camera-pairs with 1 pair referring to one camera under two adjacent rotations. Case three (Fig. 2 (c) bottomleft): we combine 7 camera-pairs in case one and 11 camera-pairs in case two, and a total of 18 camera pairs. Case four (Fig. 2 (d) bottomright): in addition to take image-pairs taken under neighboring cameras (the same rotation) and neighboring rotations (the same camera), we further take diagonal image-pairs taken under neighboring-cameras and neighboring-rotations (i.e.,  $(C_i R_j, C_{i+1} R_{j+1})$  and  $(C_i R_{j+1}, C_{i+1} R_j)$ ). At last we have 56 camera-pairs. By taking image-pairs from the chosen camera-pairs, we end up 0.42M, 0.57M, 0.99M and 3M training image-pairs in 4 cases respectively. After training, we take the trained AlexNet-type architecture out and use it to predict the object category of a test image. We have a total of 0.22M test images by split.

Implementation details: Since we have prepared training pairs for disCNN, we use the left images of training pairs as the training data for AlexNet. Therefore AlexNet and disCNN have the same number of training samples, with one image in AlexNet corresponding to an image pair in disCNN (Note: duplicate training images exist in AlexNet). To do a fair comparison, we train both AlexNet and disCNN using SGD under the same learning rate, the same number of training epochs and the same training order within each epoch. We set  $\lambda_1 = 1$  and  $\lambda_2 = 0.1$  in the objective function 1 of disCNN. Practically,  $\lambda_1$  and  $\lambda_2$  are set such that the derivatives of three separate loss terms to the parameters are at a similar scale. Both AlexNet and disCNN are trained for 20 epochs under 4 cases. The initial (final) learning rate is set to be 0.01 (0.0001), which is reduced log linearly after each epoch. The ConvNets are trained on one Tesla K40 GPU using the toolkit [29].

Results: the object recognition performances are shown in Table 1. We have the following observations: (1) disCNN consistently outperforms AlexNet under different numbers of camera pairs, with the performance gain up to  $\sim 4\%$ ; (2) when we have more camera-pairs, the performance gap between disCNN and AlexNet widens, e.g.,  $\sim 4\%$  gain under 11,18,56 camera pairs compared with  $\sim 2\%$  gain under 7 camera pairs. One potential reason is that when more camera pairs are used, more views of the same instance are available for training, therefore, a higher recognition accuracy is expected. But as observed, the performances of disCNN flatten when more camera pairs are used, e.g. the same performance under 18 and 56 camera pairs. One possible interpretation is: although we have 56 camera pairs, the diagonal camera-pairs in the case of 56 pairs do provide new pose transformation information, since the motion between a diagonal pair could be induced from motions of two camera pairs in the case of 18 pairs, a horizontal camera pair and a vertical camera pair.

Qualitative visualizations: Fig. 4 (a,b) shows the learned conv1 filters of AlexNet and disCNN in case 3, and (c,d) show their corresponding between-class confusion matrices. As seen, disCNN learns more edge-shaped filters, and disCNN improves the recognition accuracies for 8 classes, draws on one and loses one. Fig. 3 shows k nearest neighbors of the query image, based on the  $\ell_2$  distances between their fc7-identity (disCNN, 512D) and fc7 (AlexNet, 1024D) representations. We can see clearly that disCNN successfully retrieves images of the same instance under different poses as the nearest neighbors (Fig. 3 (a)). Although in some cases (Fig. 3 (b)), AlexNet find different images of the same instance as the nearest neighbors, these retrieved neighbors clearly share similar poses as the query image. These qualitative results show that disCNN disentangles the representations of identity from pose, to some extent.

## 4.2. Washington RGB-D dataset

The RGB-D dataset [17] depicts 300 common household objects organized into 51 categories. This dataset was recorded using a Kinect style 3D camera that records synchronized and aligned 640x480 RGB and depth images at 30 Hz. Each object was placed on a turntable and video sequences were captured for one whole rotation. For each object, there are 3 video sequences, each recorded with the camera mounted at a different height so that the object is viewed from different angles with the horizon. The dataset has a total of 250K images from different views and rotations. Two adjacent frames have small motions, therefore are visually very similar, and in experiments, we pick one frame from each 5 consecutive frames, resulting in  $\sim 50K$  image frames. Since the scale of the datasets does not match the scale of ConvNets, we adopt the “pretrain-finetuning”

486  
487  
488  
489  
490  
491  
492  
493  
494  
495  
496  
497  
498  
499  
500  
501  
502  
503  
504  
505  
506  
507  
508  
509  
510  
511  
512  
513  
514  
515  
516  
517  
518  
519  
520  
521  
522  
523  
524  
525  
526  
527  
528  
529  
530  
531  
532  
533  
534  
535  
536  
537  
538  
539

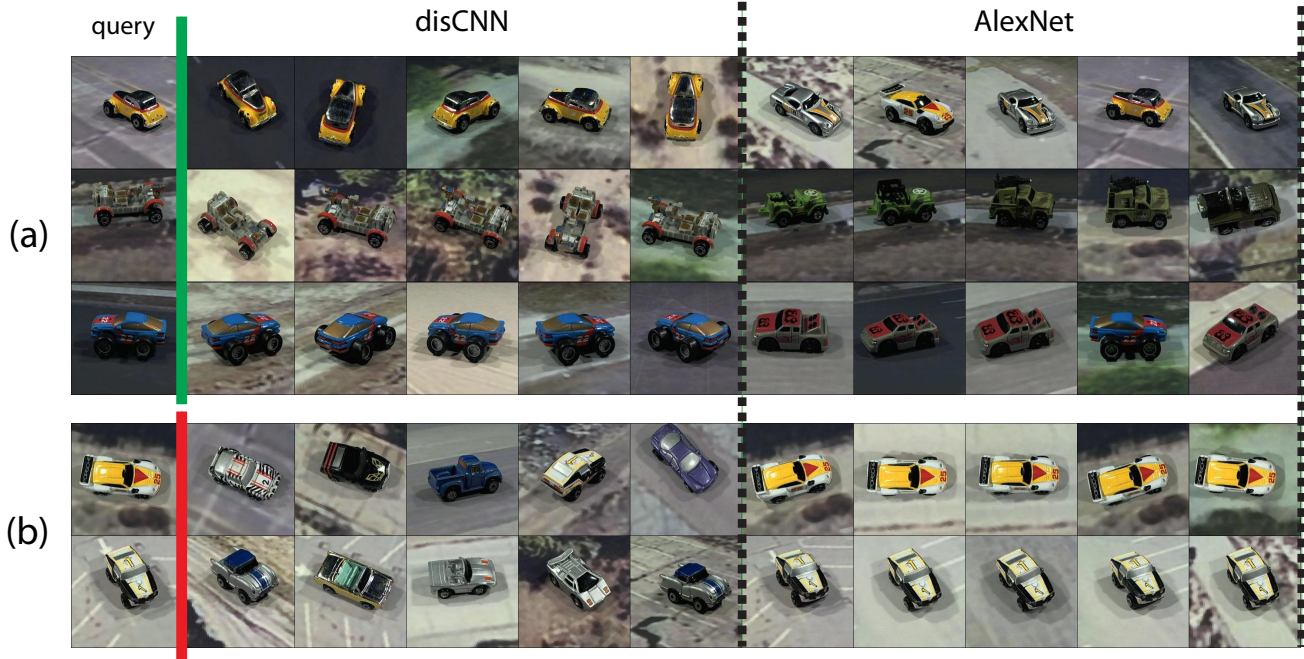


Figure 3. Examples of  $k$  nearest neighbors of query images. Images are first represented by  $fc7$ -identity (disCNN, 512D) and  $fc7$  (AlexNet, 1024D) features, and then 5 nearest neighbors are searched based on  $\ell_2$  distances in the representation spaces. On each row, the 1st image is the query image, and the next 5 (the last 5) images are retrieved nearest neighbors by disCNN and AlexNet. In group (a), disCNN always returns the same instance but under different poses as the nearest neighbors, but AlexNet fails to retrieve the same instance, instead it returns instances with different identities but similar poses. In group (b), although disCNN fails to retrieve the right instance, it does find instances with similar shapes to the query image. In this case, AlexNet retrieves the correct instances with the same identity, but again, the poses of the retrieved images are very similar to the query one. This qualitative result shows disCNN disentangles identity from pose, to some extent.

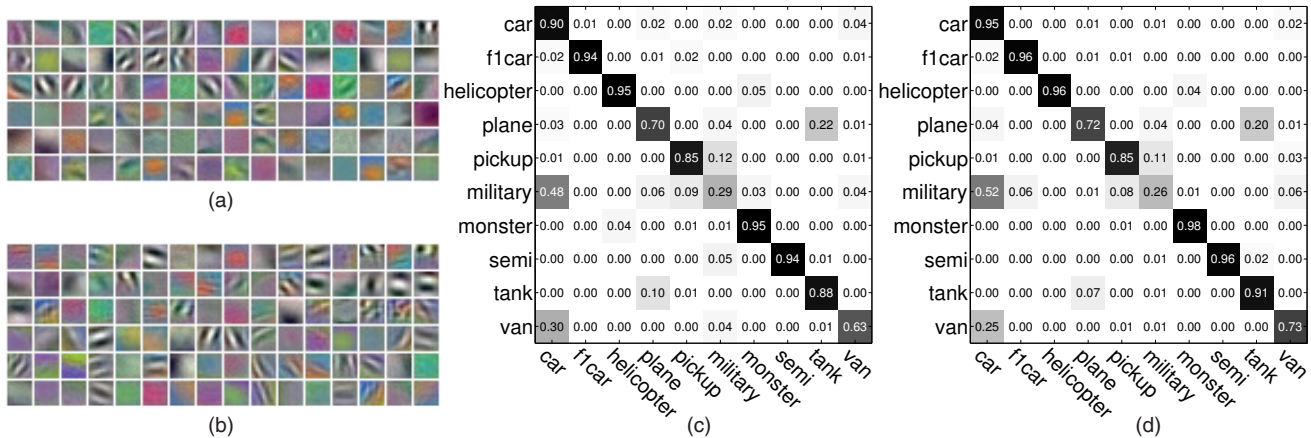


Figure 4. Learned filters and between-class confusion matrix. (a) learned Conv1 filters of AlexNet; (b) learned Conv1 filters of disCNN; between-class confusion matrix of (c) AlexNet and (d) disCNN. disCNN learns more edge-shaped filters, and improves the recognition accuracies for 8 categories (out of 10).

paradigm to do object recognition in this dataset, using the pretrained ConvNets weights on the iLab-20M dataset as initializations.

Training and test sets: [17] provided 10 partition lists of training/test. They use leave-one-out to partition: ran-

domly choose 1 instance within a category as test, and use the remaining instances as training. Due to the training time limitation, we evaluate performances using the first 3 partitions and report the mean accuracies. We use the provided object masks to crop the objects from the raw frames and

# of camera pairs	3	6	9	12	# of camera pairs	3	6	9	12
AlexNet (scratch)	71.2	72.8	72.1	72.9	AlexNet (AlexNet-iLab20M)	76.2	77.3	79.9	79.6
disCNN (scratch)	<b>75.0</b>	<b>75.1</b>	<b>77.0</b>	<b>78.6</b>	disCNN (AlexNet-iLab20M)	<b>78.9</b>	<b>80.8</b>	<b>81.5</b>	<b>82.7</b>

Table 2. Object recognition accuracies (%) of AlexNet and disCNN on the Washington RGB-D dataset. The left (right) table shows performance comparisons between disCNN and AlexNet trained from scratch (from the pretrained AlexNet features on the iLab-20M dataset). As seen, by fine-tuning CNNs from features learned on iLab-20M, large performance gains are achieved, e.g.  $\sim 4.5\%$  ( $\sim 5.5\%$ ) for disCNN (AlexNet). This shows features learned from iLab-20M are effective for, and generalizable to object recognition in the RGB-D dataset. Results from both tables shows disCNN outperforms AlexNet by  $\sim 3.5\%$  (scratch) and  $\sim 2\%$  (fine-tune), which shows the advantage of our disentangled architecture. Furthermore, when the number of camera pairs increases, the performances of disCNN increase as well.

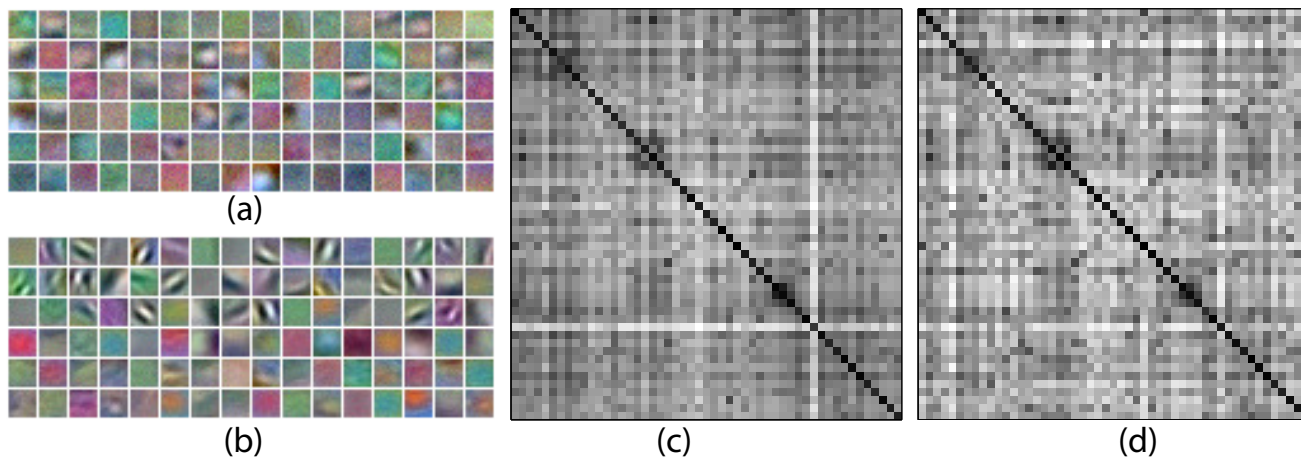


Figure 5. Learned filters and between-class  $\ell_2$  distances. (a) and (b) show the learned filters of disCNN trained from scratch, and disCNN fine-tuned from the pretrained AlexNet on the iLab-20M dataset; (c) and (d) show the between-class  $\ell_2$  distances of fc7 representations from AlexNet (1024D) and disCNN (512D). Training disCNN from scratch learns only color blobs (a). (c,d) shows visually that disCNN representations have smaller within category distances and larger between category distances. The ratio between the mean between-category distance and the mean within-category distance is 7.7/5.7 for disCNN/AlexNet.

resize them to the size  $227 \times 227$ . Since objects are located at the image center, by first cropping and then rescaling an image-pair does not change the pose-transformation of the raw pair.

Camera pairs: similarly we take different numbers of camera-pairs and evaluate influence on the performances. In one video sequence, every frame-pair with a fixed temporal gap could be imagined to be taken under a virtual camera-pair, thus all such pairs share the same pose-transformation label. As an example, two pairs,  $F_i - F_{i+\Delta}$  and  $F_j - F_{j+\Delta}$ , whose temporal gap between frames are both  $\Delta$ , then they have the same pose-transformation label. One  $\Delta$  defines one camera-pair, and in experiments, we let  $\Delta = \{5, 10, 15, 20\}$ . Case one: we take image-pairs with  $\Delta = \{5\}$  from each video sequence, and all these pairs could be thought as taken by one virtual camera pair, therefore have the same pose-transformation label. Since we have 3 video sequences, finally all pairs have in total 3 pose-transformation labels, thus equivalently 3 virtual camera pairs; Case two: take image-pairs with  $\Delta = \{5, 10\}$ ,

end in 6 camera pairs; Case three:  $\Delta = \{5, 10, 15\}$ , end in 9 camera-pairs; case four:  $\Delta = \{5, 10, 15, 20\}$ , end in 12 camera-pairs. The total number of training image pairs under each case is 67K, 99K and 131K respectively. The number of test images in all cases is 6773.

Implementation details: we use the same training settings as in iLab-20M experiments to train AlexNet and disCNN, i.e., the same learning rates (start from 0.01, end with 0.0001, with rate decreasing log linearly), the same number of training epochs (15), and the same training order within each epoch. We set  $\lambda_1 = 1$  and  $\lambda_2 = 0.05$  in experiments.

Results: we do two comparisons: first compare disCNN (AlexNet) trained from scratch against from the pretrained weights on the iLab-20M dataset, then compare disCNN against AlexNet, both fine-tuned from the pretrained CNN features on iLab-20M. Results are shown in Table 2, our observations are: (1) disCNN (AlexNet) trained by fine-tuning the pretrained AlexNet features on the iLab-20M wins over disCNN (AlexNet) trained from scratch by  $\sim 4.5\%$  ( $\sim 5.5\%$ ), and their fine-tuned performances are

756 better than the published accuracies, 74.7%, in [17] by a  
 757 large margin. This shows the features learned from the  
 758 iLab-20M dataset generalize well to the RGB-D dataset; (2)  
 759 disCNN outperforms AlexNet in both cases, either trained  
 760 from scratch or from the pretrained AlexNet features, which  
 761 shows the superiority of the disentangling architecture over  
 762 the linear chain, single task CNNs; (3) similarly, we observe  
 763 that the performance of disCNN increases as the number  
 764 of camera pairs increase. We further compute  $\ell_2$  distances  
 765 between categories using fc7-identity (disCNN, 512D) and  
 766 fc7 (AlexNet, 1024D) representations, and plot them in  
 767 Fig. 5. Visually the off diagonal elements in disCNN  
 768 are brighter and the diagonal elements are darker, show-  
 769 ing smaller within-category distances and larger between-  
 770 category distances.  
 771  
 772  
 773

### 774 4.3. ImageNet

775 ImageNet has millions of labeled images, and training a  
 776 ConvNet on a large dataset from pretrained models against  
 777 from scratch has been shown to have insignificant effects  
 778 [11, 18]. In order to show that the pretrained disCNN  
 779 on the iLab-20M datasets learns useful features for object  
 780 recognition, we fine-tune the learned weights on ImageNet  
 781 when only a small amount of labeled images are available.  
 782 We fine-tune AlexNet using 5, 10, 20, 40 images per class  
 783 (5K,10K,20K and 40K training images in total) from the  
 784 ILSVRC-2010 challenge. AlexNet is fine-tuned under three  
 785 scenarios: (1) from scratch (random Gaussian initializa-  
 786 tion), (2) from pretrained AlexNet on iLab-20M, (3) from  
 787 pretrained disCNN on iLab-20M, and top-5 object recogni-  
 788 tion accuracies are presented in Table 3. When we pretrain  
 789 AlexNet and disCNN on the iLab-20M dataset, we use the  
 790 AlexNet with the units on the last two fully connected layers  
 791 reset to 4096.  
 792  
 793

794 Results: (1) when only a limited number of labeled im-  
 795 ages are available, fine-tuning AlexNet from the pretrained  
 796 features on the iLab-20M dataset performs much better than  
 797 training AlexNet from scratch, e.g., the relative improve-  
 798 ment is as large as  $\sim 460\%$  when we have only 5 sam-  
 799 ples per class, and the improvement decreases when more  
 800 labeled images are available, but we still gain  $\sim 25\%$  im-  
 801 provements when 40 labeled images per class are available.  
 802 This clearly shows features learned on the iLab-20M dataset  
 803 generalize to ImageNet. (2) fine-tuning from the pretrained  
 804 disCNN on iLab-20M performs even better than from the  
 805 pretrained AlexNet on iLab-20M, and this shows that dis-  
 806 CNN learns even more effective features for general object  
 807 recognition than AlexNet. These empirical results show  
 808 the advantage of our disentangling architecture to the tra-  
 809 ditional single task linear architecture.

# of images/class	5	10	20	40
AlexNet (scratch)	1.47	4.15	16.45	25.89
AlexNet (AlexNet-iLab20M)	7.74	12.54	19.42	28.75
AlexNet (disCNN-iLab20M)	<b>8.21</b>	<b>14.19</b>	<b>22.04</b>	<b>30.19</b>

810 Table 3. Top-5 object recognition accuracies (%) on the test set of  
 811 ILSVRC-2010, with 150 images per class and a total of 150K test  
 812 images. First, fine-tuning AlexNet from the pretrained features on  
 813 the iLab-20M dataset clearly outperforms training AlexNet from  
 814 scratch, which shows features learned on the iLab-20M dataset  
 815 generalizes to ImageNet as well. Second, fine-tuning from the  
 816 pretrained disCNN-iLab20M performs even better than from the  
 817 pretrained AlexNet-iLab20M, which shows our disentangling archi-  
 818 tecture learns even better features for object recognition than  
 819 AlexNet.  
 820  
 821  
 822  
 823  
 824  
 825  
 826  
 827  
 828  
 829  
 830

### 831 5. Conclusions

832 In this paper, we design a multi-task learning ConvNet  
 833 to learn to predict object categories. Unlike traditional  
 834 ConvNets for object recognition, which is usually a single  
 835 task architecture and learns features sensitive to the cur-  
 836 rent task (i.e., object category) but invariant to other fac-  
 837 tors of variation as much as possible (e.g., pose), disCNN  
 838 retains all image generating factors of variation (object cat-  
 839 egory and pose transformation in our case), and learn them  
 840 simultaneously by explicitly disentangling representations  
 841 of different factors. Experiments on the large scale iLab-  
 842 20M dataset show that features learned by disCNN out-  
 843 performs features learned by AlexNet significantly for ob-  
 844 ject recognition. If we fine tune object recognition on the  
 845 ImageNet dataset using pretrained disCNN and AlexNet  
 846 features, disCNN-pretrained features are consistently bet-  
 847 ter than AlexNet-pretrained features. All experiments show  
 848 the effectiveness of our disentangled training architecture.

849 As shown in [1], features learned using egomotion as su-  
 850 pervision are useful for other vision tasks, including object  
 851 recognition, and the egomotion-pretrained features compare  
 852 favorably with features learned using class-label as supervi-  
 853 sion. In our paper, we further showed that when our model  
 854 has access to both object categories and camera motions, it  
 855 learns even better features than using only class-label as su-  
 856 pervision. One possible explanation is: although egomotion  
 857 learns useful features for object recognition, it does not nec-  
 858 essarily guarantee that feature representations of different  
 859 instances of the same class are similar since egomotion does  
 860 not has access to any class-label information. In our work,  
 861 we showed, by feeding ConvNets with additional class la-  
 862 bels, the feature learning process are further guided toward  
 863 the direction that objects of the same class tend to have spa-  
 tially similar representations.

## References

- [1] P. Agrawal, J. Carreira, and J. Malik. Learning to see by moving. In *Proceedings of the IEEE International Conference on Computer Vision*, pages 37–45, 2015. 2, 5
- [2] Y. Bengio. Learning deep architectures for ai. *Foundations and trends® in Machine Learning*, 2(1):1–127, 2009. 1, 2
- [3] A. Borji, S. Izadi, and L. Itti. ilab-20m: A large-scale controlled object dataset to investigate deep learning. In *The IEEE Conference on Computer Vision and Pattern Recognition (CVPR)*, June 2016. 4.1
- [4] L.-C. Chen, G. Papandreou, I. Kokkinos, K. Murphy, and A. L. Yuille. Semantic image segmentation with deep convolutional nets and fully connected crfs. *arXiv preprint arXiv:1412.7062*, 2014. 2
- [5] J. Deng, W. Dong, R. Socher, L.-J. Li, K. Li, and L. Fei-Fei. Imagenet: A large-scale hierarchical image database. In *Computer Vision and Pattern Recognition, 2009. CVPR 2009. IEEE Conference on*, pages 248–255. IEEE, 2009. 4
- [6] A. Dosovitskiy, J. Tobias Springenberg, and T. Brox. Learning to generate chairs with convolutional neural networks. In *Proceedings of the IEEE Conference on Computer Vision and Pattern Recognition*, pages 1538–1546, 2015. 2
- [7] R. Girshick, J. Donahue, T. Darrell, and J. Malik. Rich feature hierarchies for accurate object detection and semantic segmentation. In *Proceedings of the IEEE conference on computer vision and pattern recognition*, pages 580–587, 2014. 2
- [8] G. Gkioxari, R. Girshick, and J. Malik. Contextual action recognition with r\* cnn. In *Proceedings of the IEEE International Conference on Computer Vision*, pages 1080–1088, 2015. 2
- [9] R. Hartley and A. Zisserman. *Multiple view geometry in computer vision*. Cambridge university press, 2003. 3, 3.1
- [10] K. He, X. Zhang, S. Ren, and J. Sun. Deep residual learning for image recognition. *arXiv preprint arXiv:1512.03385*, 2015. 1, 2
- [11] G. Hinton, L. Deng, D. Yu, G. E. Dahl, A.-r. Mohamed, N. Jaitly, A. Senior, V. Vanhoucke, P. Nguyen, T. N. Sainath, et al. Deep neural networks for acoustic modeling in speech recognition: The shared views of four research groups. *Signal Processing Magazine, IEEE*, 29(6):82–97, 2012. 4.3
- [12] G. E. Hinton, A. Krizhevsky, and S. D. Wang. Transforming auto-encoders. In *Artificial Neural Networks and Machine Learning–ICANN 2011*, pages 44–51. Springer, 2011. 1
- [13] Y. Huang, W. Wang, L. Wang, and T. Tan. Multi-task deep neural network for multi-label learning. In *Image Processing (ICIP), 2013 20th IEEE International Conference on*, pages 2897–2900. IEEE, 2013. 2
- [14] S. Ioffe and C. Szegedy. Batch normalization: Accelerating deep network training by reducing internal covariate shift. *arXiv preprint arXiv:1502.03167*, 2015. 1
- [15] A. Krizhevsky, I. Sutskever, and G. E. Hinton. Imagenet classification with deep convolutional neural networks. In *Advances in neural information processing systems*, pages 1097–1105, 2012. 1, 2, 3.1
- [16] T. D. Kulkarni, W. F. Whitney, P. Kohli, and J. Tenenbaum. Deep convolutional inverse graphics network. In *Advances in Neural Information Processing Systems*, pages 2530–2538, 2015. 2
- [17] K. Lai, L. Bo, X. Ren, and D. Fox. A large-scale hierarchical multi-view rgb-d object dataset. In *Robotics and Automation (ICRA), 2011 IEEE International Conference on*, pages 1817–1824. IEEE, 2011. 4.2
- [18] Y. LeCun, Y. Bengio, and G. Hinton. Deep learning. *Nature*, 521(7553):436–444, 2015. 4.3
- [19] Y. LeCun, L. Bottou, Y. Bengio, and P. Haffner. Gradient-based learning applied to document recognition. *Proceedings of the IEEE*, 86(11):2278–2324, 1998. 1, 2
- [20] J. Long, E. Shelhamer, and T. Darrell. Fully convolutional networks for semantic segmentation. In *Proceedings of the IEEE Conference on Computer Vision and Pattern Recognition*, pages 3431–3440, 2015. 2
- [21] S. Reed, K. Sohn, Y. Zhang, and H. Lee. Learning to disentangle factors of variation with manifold interaction. In *Proceedings of the 31st International Conference on Machine Learning (ICML-14)*, pages 1431–1439, 2014. 1, 2
- [22] M. L. Seltzer and J. Droppo. Multi-task learning in deep neural networks for improved phoneme recognition. In *Acoustics, Speech and Signal Processing (ICASSP), 2013 IEEE International Conference on*, pages 6965–6969. IEEE, 2013. 2
- [23] P. Sermanet, D. Eigen, X. Zhang, M. Mathieu, R. Fergus, and Y. LeCun. Overfeat: Integrated recognition, localization and detection using convolutional networks. *arXiv preprint arXiv:1312.6229*, 2013. 2
- [24] K. Simonyan and A. Zisserman. Two-stream convolutional networks for action recognition in videos. In *Advances in Neural Information Processing Systems*, pages 568–576, 2014. 2
- [25] K. Simonyan and A. Zisserman. Very deep convolutional networks for large-scale image recognition. *arXiv preprint arXiv:1409.1556*, 2014. 1, 2, 3.1
- [26] S. Soatto, A. Chiuso, and P. Chaudhari. Visual representations: Defining properties and deep approximations. In *International Conference on Learning Representations*, volume 3, 2016. 1
- [27] H. Su, C. R. Qi, Y. Li, and L. J. Guibas. Render for cnn: Viewpoint estimation in images using cnns trained with rendered 3d model views. In *Proceedings of the IEEE International Conference on Computer Vision*, pages 2686–2694, 2015. 2, 3
- [28] C. Szegedy, W. Liu, Y. Jia, P. Sermanet, S. Reed, D. Anguelov, D. Erhan, V. Vanhoucke, and A. Rabinovich. Going deeper with convolutions. In *Proceedings of the IEEE Conference on Computer Vision and Pattern Recognition*, pages 1–9, 2015. 1, 2, 3.1
- [29] A. Vedaldi and K. Lenc. Matconvnet: Convolutional neural networks for matlab. In *Proceedings of the 23rd Annual ACM Conference on Multimedia Conference*, pages 689–692. ACM, 2015. 4.1
- [30] J. Yang, S. E. Reed, M.-H. Yang, and H. Lee. Weakly-supervised disentangling with recurrent transformations for 3d view synthesis. In *Advances in Neural Information Processing Systems*, pages 1099–1107, 2015. 2

972		1026
973	[31] C. Zhang and Z. Zhang. Improving multiview face detection	1027
974	with multi-task deep convolutional neural networks. In <i>Ap-</i>	1028
975	<i>lications of Computer Vision (WACV), 2014 IEEE Winter</i>	1029
976	<i>Conference on</i> , pages 1036–1041. IEEE, 2014. 2	1030
977	[32] Z. Zhang, P. Luo, C. C. Loy, and X. Tang. Facial landmark	1031
978	detection by deep multi-task learning. In <i>Computer Vision–</i>	1032
979	<i>ECCV 2014</i> , pages 94–108. Springer, 2014. 2	1033
980	[33] Z. Zhu, P. Luo, X. Wang, and X. Tang. Multi-view percep-	1034
981	tron: a deep model for learning face identity and view rep-	1035
982	resentations. In <i>Advances in Neural Information Processing</i>	1036
983	<i>Systems</i> , pages 217–225, 2014. 2	1037
984		1038
985		1039
986		1040
987		1041
988		1042
989		1043
990		1044
991		1045
992		1046
993		1047
994		1048
995		1049
996		1050
997		1051
998		1052
999		1053
1000		1054
1001		1055
1002		1056
1003		1057
1004		1058
1005		1059
1006		1060
1007		1061
1008		1062
1009		1063
1010		1064
1011		1065
1012		1066
1013		1067
1014		1068
1015		1069
1016		1070
1017		1071
1018		1072
1019		1073
1020		1074
1021		1075
1022		1076
1023		1077
1024		1078
1025		1079